A model of a confocal ultrasonic inspection system for interfaces

E. Yogeswaren and John G. Harris
Theoretical and Applied Mechanics, UIUC
216 Talbot Laboratory
104 South Wright Street
Urbana, IL 61801

Abstract

A mathematical model describing how a confocal arrangement of two focused ultrasonic transducers is used to interrogate a complex interface between two solid materials by scanning the focal point across the interface is outlined. A complex interface is one that has roughness and partial contact at many length scales most of which are equal to or smaller than the compressional or shear wavelength in the material. When the focused ultrasound strikes such an interface, though the focal region be small, strong multiple scattering takes place among scatterers within and adjacent to the focal region making it unclear exactly how the interface is being sampled. To clarify this issue a specific interface model consisting of multiple, small cracks having arbitrary lengths and spacings is used. This interface is interrogated by an anti-plane, focused shear wave. From this model it is possible to show that what is measured are the multiple scattered signals averaged over the aperture of the transducer, but that the dominant contribution comes from the scattered signals that phase match to the interrogating signal. Explicit expressions relating the modeled reflected and transmitted signals to the convolution of the incident wavefield with the crack-opening displacements at the focal region are given. Numerical examples are worked out for similar and contrasting materials on each side of the interface.

PACS numbers: 43.20.Gp, 43.20.Rz, 43.35.Zc

INTRODUCTION

An examination of the surfaces of a fatigue crack or a diffusion bond between contrasting metals indicates extensive regions of roughness and partial contact at many length scales. Their irregular structure significantly influences the ultrasonic signals scattered from them. The goal of this paper is to construct a model of how such an interface can be interrogated ultrasonically using a scanned, confocal arrangement of focused ultrasonic transducers and from that model to suggest what information can be extracted from the measured signals. A specific interface model consisting of multiple, small cracks having arbitrary lengths and spacings is used. This interface is interrogated by a focused anti-plane shear wave whose focal point is scanned across the interface. Definitions for the transmission and reflection coefficients measured by the transducers, constructed using a reciprocity identity, are proposed and illustrated by numerical

calculations. The assumption of anti-plane motion limits the usefulness of the model, but it is anticipated that it nevertheless captures many of the major features of the problem.

Among the several ultrasonic investigations of scattering from solid-solid interfaces formed by fatigue cracks and diffusion bonds are the following. Buck, et al.[1,2] studied the reduced probability of crack detection caused by areas of closure within the boundary of a fracture zone, while Margetan et al.[3] discussed the difficulty of detecting the presence of voids in diffusion bonded joints. More recently, Margetan, et al.[4] reported several experimental studies of scattering from various model interfaces. It seems likely that there are imperfections at many length scales at fatigue-crack tips and along diffusion bonds. However, the work cited above studied voids and asperities between 10 and 10^3 micrometers, using a confocal arrangement of focused transducers operating at approximately 10 MHz. Thompson, et al.[5] provided more specific information about the ultrasonic probes. The probes had diameters approximately 10^2 wavelengths in water and a ratio of focal length to probe diameter of approximately 7 in water. Further, Thompson, et al.[5] showed that directing the focused ultrasound into aluminium, using water as a couplant, could produce a focal region of approximately 2 compressional wavelengths in diameter, at a depth of approximately 20 compressional wavelengths into aluminium, despite strong refraction at the water-aluminium interface. The detailed structure of the wavefield in the focal region is unknown. From the earlier information, the focal region must contain no more than 10^2 scatterers, typically 10 and sometimes fewer. For example, Fig.6 of Ref.2 indicates a line image of a defect, just ahead of a fatigue crack, that is about 10 wavelengths across suggesting that it is either a large defect or a cluster of many smaller ones.

Several models, both linear and nonlinear, have been explored to estimate the scattering from an imperfect interface. Among the linear models are the following. Baik and Thompson[6] modeled a partially closed crack by replacing the crack faces by smooth surfaces and connecting the two with a distribution of linear springs. A quasi-static calculation was used to estimate the spring constants. This model was recently used, with some success, to describe the lower frequency measurements of Margetan, et al.[4]. Mikata and Achenbach[7] constructed a model of an interface using an infinite plane of randomly oriented cracks and calculated the scattering of an anti-plane shear wave. Zhang and Achenbach[8] considered adjacent cracks not necessarily lying in the same plane as a model crack system and calculated the in-plane scattering for an incident plane wave. The problem was formulated as a system of integral equations and solved numerically.

References 1 through 5 report their measurements as reflection and transmission coefficients, though it is not entirely clear what these coefficients represent.. Sotiropoulos and Achenbach[9], by considering the reflection and transmission of a normally incident longitudinal wave by a planar array of cracks, came close to defining the character of these coefficients. In their work they imagined that the wavefield scattered from the cracks was essentially plane and multiplied by a constant reflection or transmission coefficient. They extracted expressions for these coefficients in terms of the crack-opening volumes by applying the reciprocity relation to a large cell containing a portion of the infinite array of cracks. Because of the many scatterers in the cell, it is likely that, for a plane wave to dominate the propagation processes, the receiver must be in the farfield of the whole array of cracks within the cell. In this paper the authors present an alternative model that suggests that it is averaging over the transducer apertures of the various scattered signals that leads to the measured transmission and reflection coefficients and that these tranducers need only be in the farfield of an individual scatterer and not in that of the array.

The construction of the focused beam is identical to that used by Rebinsky and Harris[10] in their analysis of the line focus acoustic microscope. The scattered wavefield from the array of cracks is calculated by formulating a system of differential integral equations and solving them using a formulation used by Neerhoff[11] for a different problem. An alternative approach to formulating and solving integral equations that describe scattering from complex interfaces is described by Wickham[12]. Note also that the wavefield scattered from a periodic array of cracks, struck by a plane, anti-plane shear wave, can be estimated by approximating the dynamic nearfield with the static one[13] and calculated exactly by the Wiener-Hopf technique[14]. However, the translational symmetry of a periodic array is unlikely to be present at most interfaces so such a model can suggest misleading inferences.

I TRANSMISSION AND REFLECTION

A. Scattering of a plane wave

The plane, anti-plane shear wave

$$v_3^i = \exp[ik(x_1 \sin\eta + x_2 \cos\eta)] \tag{1}$$

INSERT FIGURE 1

is incident to the array of $(2N+1)$ cracks shown in Fig.1 at an angle η to the x_2 axis. The particle displacement v_3^i is in the x_3 direction and k is the wave number. The nth crack is $2a_n$ in length and is a distance d_n from the origin along the x_1 axis. Note that d_n is a distance with a sign. The incident wave induces a net crack opening displacement

$$[v_3] = \sum_{n=-N}^{N} [v_3]_n (x_1 - d_n, \eta) \tag{2}$$

where $[v_3]_n$ is the crack opening displacement of the nth crack. Its Fourier transform (indicated by a superscript T) is

$$[v_3]^T = \sum_{n=-N}^{N} \exp(-ik\xi d_n) a_n [v_3]_n^T (ka_n\xi, \eta) \tag{3}$$

where the (scaled) Fourier transform of the nth crack opening displacement is

$$[v_3]_n^T (ka_n\xi, \eta) = \int_{-1}^{1} [v_3]_n (a_n\chi, \eta) \exp(-ika_n\xi\chi)\, d\chi \tag{4}$$

Scattering problems of this kind can be solved either directly in the transform domain or through the intermediate step of calculating a Green's function[15]. When this is done the scattered wavefield is found to be

$$v_3 = -\frac{sgn(x_2)}{4\pi} \sum_{n=-N}^{N} ka_n \int_{-\infty}^{\infty} [v_3]_n^T (ka_n\xi, \eta) \exp[ik\xi\,(x_1 - d_n) + ik\kappa|x_2|]\, d\xi \tag{5}$$

where

$$\kappa = (1-\xi^2)^{1/2} \quad , \quad \mathrm{Im}\,\kappa \geq 0 \quad \forall\eta \tag{6}$$

The function $sgn(x)$ is plus or minus one as x is positive or negative. In several ways, one of which is indicated in Harris[16], it can be shown that provided

$$[ka_n^2 / (2\pi r_n)] << 1 \quad \forall n \tag{7}$$

where r_n is the distance from the center of the nth crack to the observation point, then Eq.(5) can be asymptotically approximated giving

$$v_3 = -\frac{sgn(x_2)}{2(2\pi)^{1/2}} e^{-i\pi/4} \sum_{n=-N}^{N} ka_n \cos\theta_n \left[v_3\right]_n^T (ka_n \sin\theta_n, \eta) \frac{\exp(ikr_n)}{(kr_n)^{1/2}} \tag{8}$$

where

$$r_n = [(x_1 - d_n)^2 + x_2{}^2]^{1/2} \quad \text{and} \quad \tan\theta_n = (x_1 - d_n) / |x_2| \tag{9a,b}$$

Figure 1 shows the various coordinates. Equation (8) represents the scattered wavefield in the farfield of any individual crack, but not in that of the array. It is interesting to note that for ka_n very small the transform can be expanded in powers of ka_n where the leading term is the quasi-static solution for the whole array. The authors believe that this is the underlying reason that the spring interface model of Baik and Thompson[6] works well at lower frequencies.

B. Scattering of a focused beam

INSERT FIGURE 2

Consider a focused beam striking the interface at a scan distance s along the x_1 axis from the origin. The geometry is indicated in Fig.2. Assume for the present that $\rho_1 = \rho_2$ and $c_1 = c_2$. Defining $y_1 = x_1 - s$, the incident focused beam is

$$u_3^i = \frac{1}{(2\pi)^{1/2}} \frac{1}{ik} \int_{-\beta}^{\beta} E(\eta) \exp[\pm ik(y_1 \sin\eta + |x_2| \cos\eta)] \, d\eta \tag{10}$$

where $E(\eta)$ and β are selected to meet an asymptotic farfield condition. The minus sign indicates a disturbance incoming to the focal plane and is used for $x_2 < 0$, while the plus sign indicates one outgoing and is used for $x_2 > 0$. The angle β is selected so that $cos\eta$ is real. Note that $\sin\eta = \xi$ and $\cos\eta = \kappa$, where κ is now restricted to be real. The details of this procedure are explained in Rebinsky and Harris[10], Eqs.(3) to (9). While there is some flexibility in the choice of $E(\eta)$ and β experience suggests that the choices

$$E(\eta) = A\exp[-(F\tan\eta)(b/g)]^{2n} \quad \text{and} \quad \pi/2 \geq \beta \geq \cot^{-1} F \tag{11a, b}$$

work well. In this case F can be interpreted as the ratio of the focal length to the aperture half width b, and A, g and m are parameters that can be chosen in several ways provided (g/b) is less than one.

To calculate the scattering of the focused beam at an interface consisting of multiple cracks, we use the linearity of the problem to relate the crack opening displacement of the nth crack for a plane wave to that of the beam by

$$[u_3]_n = \frac{1}{(2\pi)^{1/2}} \frac{1}{ik} \int_{-\beta}^{\beta} E(\eta) \exp(-iks\sin\eta)\, [v_3]_n(x_1 - d_n, \eta)\, d\eta \tag{12}$$

Therefore the beam scattered wavefield is given by Eq.(8) with v_3 replaced by u_3 and $[v_3]_n^T$ replaced by $[u_3]_n^T$, where

$$[u_3]_n^T = \frac{1}{(2\pi)^{1/2}} \frac{1}{ik} \int_{-\beta}^{\beta} E(\eta) \exp(-iks\sin\eta)\, [v_3]_n^T(ka_n\xi, \eta)\, d\eta \tag{13}$$

Accordingly, the wavefield scattered by the array of cracks, in the farfield of each individual crack, but not in that of the array, is given by

$$u_3 = -\frac{sgn(x_2)}{2(2\pi)^{1/2}} e^{-i\pi/4} \sum_{n=-N}^{N} ka_n \cos\theta_n\, [u_3]_n^T(ka_n \sin\theta_n) \frac{\exp(ikr_n)}{(kr_n)^{1/2}} \tag{14}$$

where r_n and θ_n are given by Eq.(9) and shown in Fig.1.

C. Transmission and reflection coefficients

What is measured are reflection or transmission coefficients and yet the scattered wavefield for either an incident plane wave or an incident beam does not have a structure that immediately suggests what these coefficients are. There is no single well developed wavefield transporting a slowly varying, complex amplitude characterizing transmission

and reflection. What is evident from the presence of the $(2N+1)$ propagation terms $\exp(ikr_n)$ is a scattering event from numerous, strong, compact scatterers. However, all these signals are collected by the transducers and summed in both magnitude and phase suggesting that it is the averaging effect of the transducer that gives rise to these coefficients.

Consider the confocal arrangement of two focused transducers facing one another sketched in Fig.2. The focal plane lies at the interface. The surface S_e represents the aperture emitting the incident wavefield and receiving the reflected one, while S_r represents that receiving the transmitted wavefield. An application of the reciprocity identity to the region bounded in part by these two surfaces gives

$$\int_{S_r} (u_3^2 \tau_{32}^1 - u_3^1 \tau_{32}^2)\, dx_1 - \int_{S_e} (u_3^2 \tau_{32}^1 - u_3^1 \tau_{32}^2)\, dx_1 = \sum_{n=-N}^{N} \int_{-a_n}^{a_n} [u_3]_n (x_1 - d_n)\, \tau_{32}^1\, dx_1 \qquad (15)$$

where wavefield 2 has been selected to be the incident plus scattered beam wavefield and 1 is as yet unspecified. In deriving this identity, it is assumed that the wavefields outside the surfaces S_r and S_e are negligible and that none of the scattered radiation collected by S_r and S_e is reflected back. The first condition can be approximated by using a well-collimated beam and noting that the surfaces containing S_r and S_e are in the farfield of any individual crack. Further, the array of cracks is bounded so that the scattered waves decay geometrically far from the ends of the array. The second condition can be approximated by assuming that a tone burst is used and that all but the initially arriving signals are gated out.

Consider transmission. For wavefield 1 the beamfield

$$u_3^1 = \frac{-1}{(2\pi)^{1/2}} \frac{1}{ik} \int_{-\beta}^{\beta} E^*(\eta) \exp[\mp ik(y_1 \sin\eta + |x_2| \cos\eta)]\, d\eta \qquad (16)$$

is chosen, where the asterisk indicates the complex conjugate. Physically this represents a beam going in the opposite direction to that of the incident beam. The minus sign indicates a wavefield incoming to the focal plane and is used for $x_2 > 0$, while the plus sign is used for a wavefield outgoing from the focal plane and is used for $x_2 < 0$. The stress $\tau_{32} = \mu\, \partial_2 u_3$ for both wavefields 1 and 2. Evaluating the right hand side of Eq.(15) gives

$$\int_{S_r}(\ldots)-\int_{S_e}(\ldots)=\frac{\mu}{(2\pi)^{1/2}}\sum_{n=-N}^{N}a_n\int_{-1}^{1}[u_3]_n(a_n\chi)\,F^*(a_n\chi+d_n-s)\,d\chi \tag{17}$$

where, after scaling the integration variable,

$$F(x)=\int_{-\beta}^{\beta}E(\eta)\cos\eta\,\exp(ikx\sin\eta)\,d\eta \tag{18}$$

A suitable $E(\eta)$ is given by Eq.(11). Note that $E(\eta)$ is an even function so that the exponential in the integral Eq.(18) can have either a plus or minus sign. We have chosen the plus sign. Further note that $F(x)$ is essentially the Fourier transform of $E(\eta)$. If the interrogating system is well designed, then $F(a_n\chi+d_n-s)$ will be sharply peaked near $d_n=s$. If the nth crack were large enough to occupy the focal region, then Eq.(17) indicates that indeed it is the nth crack that is being interrogated. Further, note that even though only the crack opening displacements within the focal region are directly detected their magnitude and phase is a consequence of the a multiple scattering among all the cracks of the array. How many cracks participate is not clear, though intuition suggests that only those adjacent to the focal region are important.

To evaluate the integrals on the left side of Eq.(15) approximate expressions for wavefields 1 and 2 at S_r and S_e are needed. Asymptotically approximating Eq.(16), wavefield 1 becomes

$$u_3^1(\mathbf{x})=\frac{i}{k}\,\frac{E^*(\theta)}{(kr)^{1/2}}\,e^{\pm i\pi/4}\,e^{\mp ikr} \tag{19}$$

The corresponding τ_{32}^1 is gotten from Eq.(19) by multiplying it by $(-i\mu\cos\theta)$. The coordinates (r,θ) are

$$r=(y_1^{\,2}+x_2^{\,2})^{1/2}\quad\text{and}\quad\tan\theta=y_1/|x_2| \tag{20a,b}$$

INSERT FIGURE 3

and are shown in Fig.3 along with the related crack coordinates (r_n,θ_n). Recall that $y_1=x_1-s$. Figure 3 is drawn assuming identical materials on each side of the interface.

Equation (14) added to the incident wavefield provides wavefields 2 at the transducer faces. However it is useful to write these expressions in a way that explicitly exhibits the pointwise transmission and reflection coefficients. For transmission, $x_2>0$, wavefield 2 is written as

$$u_3^2(\mathbf{x}) = T(\mathbf{x}) \frac{1}{ik} \frac{E(\theta)}{(kr)^{1/2}} \quad e^{-i\pi/4} \; e^{ikr} \tag{21}$$

The term $T(\mathbf{x})$ is a pointwise transmission coefficient and is given by

$$T(\mathbf{x}) = 1 - \frac{ik}{2(2\pi)^{1/2}} \frac{1}{E(\theta)} \sum_{n=-N}^{N} ka_n \cos\theta_n \left[u_3\right]_n^T (ka_n \sin\theta_n)(\frac{r}{r_n})^{1/2} e^{ik(r_n - r)} \tag{22}$$

The propagation terms vary rapidly over the aperture of the transducer unless the observation point is very far from the scatterers making $r \approx r_n$. This is not the case here and accordingly the propagation terms cannot be dropped. Note that the pointwise coefficient, in principle, has contributions from all $(2N+1)$ scatters. The corresponding τ_{32}^2 is given, to the same order of approximation, by

$$\tau_{32}^2 = \mu \cos\theta \, T(\mathbf{x}) \frac{E(\theta)}{(kr)^{1/2}} \quad e^{-i\pi/4} \; e^{ikr} + \mu \frac{\partial T}{\partial x_2} \frac{1}{ik} \frac{E(\theta)}{(kr)^{1/2}} \quad e^{-i\pi/4} \; e^{ikr} \tag{23}$$

Note that the derivative cannot be dropped because it will contain a term proportional to $k(r - r_n)$ that is not always of higher order, in powers of $(kr)^{-1/2}$ or $(kr_n)^{-1/2}$, than those retained. The reflected wavefield 2 has a similar form, namely,

$$u_3^2(\mathbf{x}) = \frac{1}{ik} \frac{E(\theta)}{(kr)^{1/2}} \quad [e^{i\pi/4} e^{-ikr} + R(\mathbf{x}) e^{-i\pi/4} e^{ikr}] \tag{24}$$

The pointwise reflection coefficient $R(\mathbf{x})$ is given by

$$R(\mathbf{x}) = 1 - T(\mathbf{x}) \tag{25}$$

This relationship reflects the inherent odd reflection symmetry in the scattering problem. Again a derivative $\partial R / \partial x_2$ appears in the calculation of τ_{32}^2 and cannot immediately be discarded.

Expressions (19) to (25) are substituted into Eq.(15) and the resulting integrals estimated asymptotically, though detailed estimates are not needed. The derivative term in Eq.(23) makes no contribution to leading order in the integral over S_r because its saddle point contribution is zero. The saddle point occurs for $r = r_n$ and $\theta = \theta_n$ Expressed physically it means that the leading order contribution comes only from those crack-scattered waves that phase match to the dominant incident term. Elsewhere over the transducer aperture destructive interference takes. No saddle point lies in the interval of integration when estimating the integral over S_e. The end point contributions are all of lower order. These considerations lead to the following definition of a generalized transmission coefficient **T**, namely

$$\mathbf{T} = \frac{1}{P}\int_{-\beta}^{\beta} T(\mathbf{x})E(\eta)E^*(\eta)\,d\eta \tag{26}$$

where

$$P = \int_{-\beta}^{\beta} E(\eta)E^*(\eta)\,d\eta \tag{27}$$

Lastly, from Eqs.(15) to (26), **T** is given by

$$\mathbf{T} - 1 = \frac{ik}{2(2\pi)^{1/2}}\frac{1}{P}\sum_{n=-N}^{N} ka_n \int_{-1}^{1} [u_3]_n(a_n\chi)\, F^*(a_n\chi + d_n - s)\,d\chi \tag{28}$$

where $F(x)$ is given by Eq.(18). The crack opening displacements $[u_3]_n$ are calculated numerically. The procedure is indicated in Sec. III.

An argument quite analogous to that just given using as wavefield 1

$$u_3^1 = \frac{-1}{(2\pi)^{1/2}}\frac{1}{ik}\int_{-\beta}^{\beta} E^*(\eta)\exp[\pm ik(y_1\sin\eta + |x_2|\cos\eta)]\,d\eta \tag{29}$$

where the plus sign is used for $x_2 > 0$ and the minus sign for $x_2 < 0$, leads to a definition of the generalized reflection coefficient **R** that is identical to that of **T** if $T(\mathbf{x})$ is replaced by $R(\mathbf{x})$. Moreover, it is readily shown that

$$\mathbf{R} = 1 - \mathbf{T} \tag{30}$$

Using an electromechanical reciprocity relation and an argument similar to Auld's[17], it is possible to show that the generalized transmission and reflection coefficients are proportional, at a given angular frequency ω, to the corresponding model voltages. Equations (28) and (30) capture the idea of one dimensional imaging of the interface. The transducers and lens are designed to make $F(x)$ as narrow as possible so that the measured coefficients are responding only to those scatterers near the scanning position s. To make $F(x)$ narrow the apertures must be large. Correspondingly, averaging over the transducer apertures means that the dominant contribution comes from those scattered signals that constructively interfere with the incident signal. Lastly, note the convolution structure of the integrals of Eq.(28) suggesting that a deconvolution of $\mathbf{T}$ and $\mathbf{R}$ might give the crack opening displacements.

II AN INTERFACE BETWEEN CONTRASTING MATERIALS

The work of the previous section is readily extended to the case in which the materials on each side of the interface are contrasting. Figure 2 shows the overall geometry. A number of details will be omitted here because they are quite close to those of the previous section. Some are given in Yogeswaren[18].

When a focused beam is refracted at the interface into a faster material the beam may spread rapidly and some components of its angular spectrum may experience critical refraction. Accordingly, the aperture collecting the transmitted signal may only intercept a small fraction of the transmitted beam. To avoid these problems it will be assumed that the beam is always refracted into the slower material. That, in combination with limiting the angular spectrum of the beam in the incident material to real angles, implies that all the plane wave reflection and transmission coefficients for the defect-free interface discussed next are real.

A. Transmission and reflection coefficients

Firstly, consider an interface with no cracks present. Material 2 is that for $x_2 < 0$ and 1 that for $x_2 > 0$ (Fig.2). The reflection coefficient for a plane wave incident at an angle η from 2, $R_{22}(\eta)$, is

$$R_{22}(\eta) = A_{-}(\eta) / A_{+}(\eta) \tag{31}$$

and the transmission coefficient from 2 to 1, $T_{21}(\eta)$, is

$$T_{21}(\eta) = [A_{-}(\eta) + A_{+}(\eta)]/A_{+}(\eta) \tag{32}$$

The $A_{\pm}(\eta)$ are

$$A_{\pm}(\eta) = (\rho_2 c_2/\rho_1 c_1)\cos\eta \pm a(\eta) \tag{33}$$

where

$$a(\eta) = [1-(c_1/c_2)^2 \sin^2\eta]^{1/2} \tag{34}$$

Note that $a(\eta)$ is real because c_1/c_2 is restricted to be less than one and η is restricted to real values.

The focused beam incident from material 2 is given, in $x_2 < 0$, by Eq. (10) with k replaced by k_2, where $k_2 = \omega/c_2$ and β replaced by β_2. The value of β_2 is suggested by Eqs.(11a,b). The transmitted beam, in $x_2 > 0$, is given by

$$u_3^t = \frac{1}{(2\pi)^{1/2}} \frac{1}{ik_2} \int_{-\beta_2}^{\beta_2} E(\eta)\, T_{21}(\eta) \exp[ik_1(y_1 \sin\gamma + |x_2|\cos\gamma)]\, d\eta \tag{35}$$

The angles η and γ are related by

$$\sin(-\eta)/c_2 = \sin\gamma/c_1 \tag{36}$$

The minus sign arises from the sign convention that is used to construct the incident and refracted focused beams. The reflected beam, in $x_2 < 0$, is given by

$$u_3^r = \frac{1}{(2\pi)^{1/2}} \frac{1}{ik_2} \int_{-\beta_2}^{\beta_2} E(\eta)\, R_{22}(\eta) \exp[ik_2(y_1 \sin\eta + |x_2|\cos\eta)]\, d\eta \tag{37}$$

The transmitted traction τ_{32}^t at the interface when no cracks are present is

$$\tau_{32}^t = \mu_1 F^t(y_1)/(2\pi)^{1/2} \tag{38}$$

where

$$F^t(x) = \frac{c_2}{c_1} \int_{-\beta_2}^{\beta_2} E(\eta)\, T_{21}(\eta) a(\eta) \exp(ik_2 x \sin\eta)\, d\eta \tag{39}$$

and $\mu_1 = \rho_1 c_1^2$. The continuity of traction means that τ_{23}^t equals the sum of the incident and reflected tractions $\tau_{23}^i + \tau_{23}^r$. Note that both $E(\eta)$ and $T_{21}(\eta)$ are symmetric in η.

B. Transmission and reflection coefficients

Generalized transmission and reflection coefficients are again defined and calculated using the reciprocity identity, Eq.(15). The generalized transmission coefficient is given by

$$\mathbf{T}_{21}^c - \mathbf{T}_{21} = \frac{ik_2}{2(2\pi)^{1/2}} \frac{1}{P} \sum_{n=-N}^{N} k_2 a_n \int_{-1}^{1} [u_3]_n(a_n\chi)\, F^{t*}(a_n\chi + d_n - s)\, d\chi \tag{40}$$

where P is given by Eq.(27) and F^t by Eq.(39). Recall that the asterisk indicates the complex conjugate. The transmission coefficient $\mathbf{T}_{21}^c$ is that measured when imperfections are present at the interface and is defined by

$$\mathbf{T}_{21}^c = \frac{1}{P} \int_{-\beta_2}^{\beta_2} T_{21}^c(\mathbf{x}) E(\eta) E^*(\eta) \frac{c_2 a(\eta)}{c_1 \cos\eta}\, d\eta \tag{41}$$

where $T_{21}^c(\mathbf{x})$ is a pointwise coefficient similar that of Eq.(22). The coefficient $\mathbf{T}_{21}$ is that for a defect-free interface and is defined by

$$\mathbf{T_{21}} = \frac{1}{P}\int_{-\beta_2}^{\beta_2} T_{21}(\eta)E(\eta)E^*(\eta)\frac{c_2 a(\eta)}{c_1\cos\eta}\,d\eta \tag{42}$$

where $T_{21}(\eta)$ is given by Eq.(32). The ratio $[c_2 a(\eta)/c_1\cos\eta]$ is a consequence of Snell's law, Eq.(36), and takes account of the different rates of spreading in the two contrasting materials. The generalized reflection coefficient $\mathbf{R^c_{22}}$ is defined by

$$\mathbf{R^c_{22}} = \frac{1}{P}\int_{-\beta_2}^{\beta_2} R^c_{22}(\mathbf{x})\,E(\eta)E^*(\eta)\,d\eta \tag{43}$$

where $R^c_{22}(\mathbf{x})$ is the pointwise coefficient. The coefficient $\mathbf{R^c_{22}}$ is calculated just as was $\mathbf{T^c_{21}}$ and is given by

$$\mathbf{R^c_{22}} - \mathbf{R_{22}} = (\rho_1 c_1^{\,2}/\rho_2 c_2^{\,2})(\mathbf{T_{21}} - \mathbf{T^c_{21}}) \tag{44}$$

where the coefficient $\mathbf{R_{22}}$ for a defect free interface is given by Eq.(43) with $R^c_{22}(\mathbf{x})$ replaced by $R_{22}(\eta)$, Eq.(31). Note that the expressions for the generalized coefficients arise from both a refraction and reflection problem, and a scattering problem.

III THE VECTOR DIFFERENTIAL INTEGRAL EQUATION

It remains to calculate the crack opening displacements. Consider the case of contrasting materials. The case of similar materials follows from this. Firstly, remove the geometrical wavefield existing when no cracks are present and formulate a boundary value problem for the scattered wavefields in each material. Secondly, note that the traction across the interface is continuous, but that the particle displacement changes discontinuously across each crack. Lastly, note that the scattered traction on the crack faces equals the negative of the tractions generated by the geometrical wavefield. From this a system of differential integral equations can be formulated that can be solved numerically. The method follows that used by Neerhoff[11]. The vector equation is given by

$$\frac{1}{2(2\pi)^{1/2}}\left[\partial_2\int_{-1}^{1}\mathbf{K}(\eta,\gamma)\cdot\mathbf{U}(\gamma)\,d\gamma\right]_{x_2=0} = \mathbf{I}(\eta), \quad -1\le\eta\le 1 \tag{45}$$

where the derivative is left outside the integral for the present . The mth component of the source vector $\mathbf{I}(\eta)$ containing the geometrical wavefield is

$$I_m(\eta) = -F^t(a_m\eta + d_m - s) \tag{46}$$

where $F^t(x)$ is given by Eq.(39). The nth component of the vector $\mathbf{U}(\gamma)$ containing the crack opening displacements is

$$U_n(\gamma) = [u_3]_n(a_n\gamma) \tag{47}$$

where $[u_3]_n$ is defined in Eq.(12) and is unknown. The mnth component of the kernel tensor $\mathbf{K}(\eta,\gamma)$ is

$$K_{mn}(\eta,\gamma) = k_2 a_n \int_{-\infty}^{\infty} \frac{2\kappa_2\, d\xi}{[(\rho_1 c_1/\rho_2 c_2)\kappa_1 + \kappa_2]} \times \exp[ik_2\xi(a_m\eta + d_m - a_n\gamma - d_n)]e^{ik_2(c_2/c_1)\kappa_1 x_2} \tag{48}$$

The radical κ_2 is identical to κ given by Eq.(6). The radical κ_1 is

$$\kappa_1 = [1-(c_1/c_2)^2\xi^2]^{1/2} \quad \text{Im}\,\kappa_1 \geq 0 \quad \forall\xi \tag{49}$$

and is essentially the same as the function $a(\eta)$, Eq.(34).

To solve Eq.(45) the $U_n(\gamma)$ are approximated over the interval $(-1 \leq \gamma \leq 1)$ by an expansion in P Chebyshev polynomials $\phi_p(\gamma)$. That is

$$U_n(\gamma) \approx \sum_{p=1}^{P} C_n(p)\phi_p(\gamma) \tag{50}$$

where

$$\phi_p(\gamma) = \begin{cases} i\sin[p\,\sin^{-1}(\gamma)] & p = 2,4,6,\ldots \\ \cos[p\,\sin^{-1}(\gamma)] & p = 1,3,5,\ldots \end{cases} \tag{51a, b}$$

and the coefficients $C_n(p)$ are unknown. Note that each polynomial behaves as $(1\pm\gamma)^{1/2}$ near $\gamma=\mp1$ so that the edge condition for each individual crack is satisfied. Both sides of Eq.(45) are multiplied by a member of the P ϕ_p and Eq.(50) is used giving

$$C_n(p)\left[\partial_2\int_{-1}^{1}d\eta\int_{-1}^{1}d\gamma\;\phi_q(\eta)\;K_{\mathrm{mn}}(\eta,\gamma)\;\phi_p(\gamma)\right]_{x_2=0}=\int_{-1}^{1}d\eta\;\phi_q(\eta)\;I_{\mathrm{m}}(\eta) \tag{52}$$

where a summation over n and p is implied. The integrations in γ and η are interchanged with that in ξ in Eq.(48) and then performed. This is followed by interchanging the derivative and the integration over ξ and evaluating the integrand at $x_2=0$. By performing the operations in this order the singularity that would arise from interchanging the two operations at an earlier stage has been avoided. Accordingly, the differential integral equation has been reduced to the following system of algebraic equations.

$$A_{mn}(q,p)\,C_n(p)=V_m(q) \tag{53}$$

where

$$A_{mn}(q,p)=\frac{-ik_2\pi}{2(2\pi)^{1/2}}\,qp\int_0^{\infty}\frac{d\xi}{\xi^2}\,\frac{2\kappa_1\kappa_2[e^{ik_2d_{mn}\xi}+(-1)^q(-1)^pe^{-ik_2d_{mn}\xi}]}{[(\rho_1c_1/\rho_2c_2)\kappa_1+\kappa_2]}\,J_q(k_2a_m\xi)\,J_p(k_2a_n\xi) \tag{54}$$

and

$$V_m(q)=q\int_0^{\xi_2}\frac{d\xi}{\xi(1-\xi^2)^{1/2}}\,E(\eta)\,T_{21}(\eta)\,a(\eta)\,J_q(k_2a_m\xi)\times[e^{ik_2\xi(d_m-s)}-(-1)^qe^{-ik_2\xi(d_m-s)}] \tag{55}$$

The indices m,n = -N,..., -2, -1, 0, 1, 2, ..., N and the indices q,p = 1, 2, ..., P. The first set of indices indicate the mth and nth cracks, respectively. Thus $A_{mn}(q,p)$ is the qth row and pth column of the submatrix positioned at the mth row and nth column of the global matrix, $C_n(p)$ is the pth row of the Chebyshev coefficient subvector at the nth row of the global vector and $V_m(q)$ is the qth row of the source subvector at the mth row of the global source vector. The distance $d_{mn}=d_m-d_n$. In Eq. (55)

$$\eta = \sin^{-1}\xi \quad \text{and} \quad \xi_2 = \sin\beta_2 \tag{56a,b}$$

Though the numerical procedure is straightforward it is important to try to assess its accuracy and correctness by comparing its predictions with a known result. In the Appendix the same numerical procedure is used to calculate the reflection coefficient for a plane wave normally incident to a coplanar periodic array of cracks. While this problem does not allow all aspects of the numerical work to be checked, the good agreement between the numerical predictions and the known analytical ones suggests that the procedure is accurate.

IV NUMERICAL EXAMPLES

INSERT FIGURES 4 AND 5

Figure 4 shows the transverse profiles of the incident, and scattered beams for two contrasting materials. The magnitude $|k_2 u_3|$ is plotted against $\bar{y}_1 = y_1 / b$. The u_3 symbolizes whatever displacement term is being discussed. The focused beam is characterized by setting $\beta_2 = \cot^{-1} F$, $A = (2\pi)^{1/2} / (2\beta_2)$, $F = 1$, $g / b = 0.75$ and $k_2 b = 40$. The materials are characterized by the ratios $c_2 / c_1 = 1.33$ and $\rho_2 c_2 / \rho_1 c_1 = 1.34$. These material constants are typical of a nickel copper combination. The solid line indicates the incident wavefield at $\bar{x}_2 = -1$,where $\bar{x}_2 = x_2 / f$ and f is the imagined focal length, the long dashed line indicates the reflected wavefield at the same location and the short dashed line with the broader profile indicates the transmitted wavefield at $\bar{x}_2 = 1$. The narrow profile with side lobes given by the short dashed line indicates the profile in the focal plane. The focal region is on the order of $0.4b$ wide. The beam spreads more slowly in the slower material, as expected. Figure 5 shows a profile of the beam along its central axis for $k_2 b = 100$. The remaining parameters are identical to those of Fig.4. Here the magnitude of the net normalized displacement is plotted against $\bar{x}_2$. The focal region extends over $0.4f$. Because $F = f / b$ and $F = 1$, increasing $k_2 b$ by a factor of the order of 2 will decrease the width and length of the focal region by approximately 1/2. The focal region is about 2 times longer than it is wide. The beam parameters given here will be used for the following figures.

INSERT FIGURES 6 AND 7

Figure 6 shows an interface between identical materials. There are three zones containing cracks of different sizes. Zone Z1 contains 5 equal cracks. The length of each crack and the spacing between adjacent cracks is $2a$, and $\bar{a} = 0.1$ where $\bar{a} = a / b$. Zone Z2 is identical to Z1 except that $\bar{a} = 0.15$. Zone Z3 consists of one crack with $\bar{a} = 1$. The interaction among the scatterers is likely to be strong for they are immediately adjacent to one another. Nevertheless the cracks tips are closed. In each case two scans are undertaken. The solid line indicates that for $k_2 b = 40$ and the dashed line indicates that for $k_2 b = 100$. Figure 7 shows the magnitude of $\mathbf{R}$ plotted against $\bar{s}$, where $\bar{s} = s / b$. The corresponding value of $\mathbf{T}$ is readily deduced from Eq.(30).

INSERT FIGURES 8, 9 AND 10

Figure 8 shows an interface between contrasting materials having the same ratios of materials properties as those used for Fig.4. The arrangement of cracks is symmetric, with the largest crack at the center. The half-width of the cracks is given by $\bar{a}_n = 0.5 - 0.1n$ and the distance to each crack is given by $|\bar{d}_n| = |\bar{d}_{n-1}| + \bar{a}_n + \bar{a}_{n-1} + 0.001$, where $\bar{d}_n = d_n / b$. Figure 9 shows $|\mathbf{T}^c_{21} - \mathbf{T}_{21}|$ and Fig.10 shows $|\mathbf{T}^c_{21}|$ both plotted against $\bar{s}$ for this interface. From Eq.(44) the corresponding value of $|\mathbf{R}^c_{22} - \mathbf{R}_{22}|$ can be deduced.

V CONCLUSIONS

Examining Figs.6 and 7 neither the $k_2 b = 40$ scan nor the $k_2 b = 100$ scan is able to resolve the structure of the cracks of Z1 and Z2. In both cases the cracks of Z1 and Z2 give a reflection coefficient suggesting only one crack. Moreover, the $k_2 b = 100$ scan almost seems to resolve only one crack. Accordingly, though the cracks of Z2 were approximately the same width as the focal region of the $k_2 b = 100$ scan the closed crack tips are not evident. Examining Figs.8,9 and 10 indicates that the $k_2 b = 40$ scan does not resolve the cracks, but rather it suggests only the presence of three larger cracks all of approximately the same size. However, the $k_2 b = 100$ scan does resolve all but the smallest cracks at the ends of the array. In this case the focal width is less than all but the smallest cracks. Lastly, note that the interfaces examined are all ones for which strong interactions among the cracks are anticipated so that the clusters of smaller cracks act as single scatterers.

In summary, a mathematical model describing how a confocal arrangement of two focused ultrasonic transducers can be used to interrogate a complex interface between two solid materials by scanning the focal point across the interface has been outlined. The central hypothesis was that averaging over the transducer apertures yielded approximations to the measured transmission and reflection coefficients and that these coefficients were a consequence of multiple scattering processes. Expressions relating the measured coefficients to the scatters were derived. Equations (28) and (40) constitute the principle theoretical results. The convolutions evident on the right hand sides of these equations suggest that a deconvolution of the measured coefficients could yield information about the scatterers. The numerical examples indicate the difficulty in determining the detailed structure a complex interface.

ACKNOWLEDGMENT

This work is supported by the National Science Foundation through Grant No. MSS - 9114547. Additional computational support was provided by NCSA Grant No. CEE - 920021N.

APPENDIX: Plane wave scattering from a periodic array

Consider a plane wave, of unit amplitude, normally incident to the array of $(2N+1)$ cracks between identical materials shown in Fig.2. Set a_n to a and d_n to nd for all n, giving a finite periodic array. There is no real aperture in this problem so that a slightly different definition of a reflection coefficient needs to be used. Following Harris and Yogeswaren[19] define a reflection coefficient as

$$\mathbf{R} = -\frac{a}{2d}\frac{1}{(2N+1)}\sum_{n=-N}^{N}\int_{-1}^{1}[v_3]_n(a\chi,0)\,d\chi \tag{58}$$

where the $[v_3]_n$ are given by Eq.(2) with $\eta = 0$. For a finite array the $[v_3]_n$ will not be identical, but, as N becomes large, they should approach a constant value.

Lamb[13] gives an approximate solution for the reflection coefficient for a plane wave normally incident to an infinite periodic array of cracks that is accurate for small *kd*. That coefficient is

$$\mathbf{R} = \frac{-ikl}{1-ikl} \tag{59}$$

where

$$l = \frac{d}{\pi}\ln[\sec(\pi a / d)] \tag{60}$$

A comparison of the two problems indicates that as N becomes large the reflection coefficient defined by Eq.(58) should closely approximate that defined by Eq.(59) for a small *kd*. Figure 11 shows a comparison of the magnitudes of the two coefficients for a range of *ka* and $d/a = 2.5$. The dashed line indicates the $\mathbf{R}$ from Eq.(59) and the solid line that from Eq.(58). Equation (58) was evaluated by increasing N until the difference between the Nth and the $(N-1)$th terms was negligible. The agreement between the two is satisfactory.

REFERENCES

[1] O. Buck, R.B. Thompson, and D.K. Rehbein, J. Nondestr. Eval. **4**, 203-212 (1984).

[2] O. Buck, D.K. Rehbein and R. B. Thompson, Engng. Fracture Mech. **28**, 413-424 (1987).

[3] F.J. Margetan, R.B. Thompson and T.A. Gray, J. Nondestr. Eval. **7**, 131-152 (1988).

[4] F.J. Margetan, R.B. Thompson, J.H. Rose and T.A. Gray, J. Nondestr. Eval. **11**, 109-26 (1992).

[5] R.B. Thompson, C.J. Fiedler and O. Buck, in *Nondestructive Methods for Material Property Determination*, edited by C.O. Rund and R.E. Green (Plenum, New York, 1984) pp. 161-170.

[6] J.-M. Baik and R.B. Thompson, J. Nondestr. Eval. **4**, 177-96 (1979).

[7] Y. Mikata and J.D. Achenbach, J. Acoust. Soc. Am. **83**, 38-45 (1988).

[8] Ch. Zhang and J.D. Achenbach, J. Appl. Mech. **55**, 104-110 (1988).

[9] D.A. Sotiropoulos and J.D. Achenbach, J. Acoust. Soc. Am. **84**, 752-9 (1988).

[10] D.A. Rebinsky, and J.G. Harris, Proc. R. Soc. Lond. A**436**, 251-265 (1992).

[11] F.L. Neerhoff, Appl. Scientific Res. **35**, 237-249 (1979).

[12] G. Wickham, J. Nondestr. Eval.. **11**, 199-210 (1992).

[13] H. Lamb, *Hydrodynamics*, 6th ed. (Dover, New York, 1945), pp. 533-538.

[14] L.A. Weinstein, *The Theory of Diffraction and the Factorization Method* (Golem, Boulder, CO, 1969), pp.267-281.

[15] P.M. Morse and H. Feshbach, *Methods of Theoretical Physics* (McGraw-Hill, New York, 1953), pp.803-833 and pp. 1360-1364.

[16] J.G. Harris, J. Acoust. Soc. Am. **82**, 635-646 (1987).

[17] B.A. Auld, Wave Motion **1**, 3-10 (1979).

[18] E. Yogeswaren, *Scattering from Imperfect Interfaces* (Ph.D. Thesis, UIUC, Urbana,IL, 1994).

[19] J. G. Harris and E. Yogeswaren, Appl. Mech. Rev., to appear (1993)

Figure captions for

A model of a confocal ultrasonic inspection system for interfaces by E. Yogeswaren and J.G. Harris

Figure 1. The $(2N+1)$ cracks, indicating the geometrical parameters for the plane wave and focused beam scattering.

Figure 2. The geometry of the focused beam scanning the interface. The case for contrasting materials is shown.

Figure 3. The geometry of the focused beam scattering the interface. The crack based coordinates are contrasted with those based at the focal point. The case for similar materials is shown.

Figure 4. Transverse profiles of the incident, and scattered beams for $kb = 40$. $c_2 / c_1 = 1.33$. $\rho_2 c_2 / \rho_1 c_1 = 1.34$. Solid line the incident beam. Long dashed line the reflected beam. Short dashed line the transmitted beam. Short dashed line with sidelobes the beam at the interface.

Figure 5. Longitudinal profile of the net normalized displacement beam along the beam's axis for $kb = 100$. The material ratios are identical to those used in Fig.4.

Figure 6. An interface between identical materials. Z1 contains 5 equal cracks, $\bar{a} = 0.1$. Z2 is identical to Z1 with $\bar{a} = 0.15$. Z3 contains one crack with $\bar{a} = 1$.

Figure 7. The magnitude $\mathbf{R}$ for the interface of Fig.6 plotted against $\bar{s}$.

Figure 8. An interface between the contrasting materials. The $\bar{a}_n$ become progressively smaller as indicated. The magnitude of the $\bar{d}_n$ is also indicated.

Figure 9. The magnitude $|\mathbf{T}^c_{21} - \mathbf{T}_{21}|$ for the interface of Fig.8 plotted against $\bar{s}$. The material ratios are identical to those used in Fig.4.

Figure 10. The magnitude $|\mathbf{T}^c_{21}|$ plotted against $\bar{s}$. The parameters are identical to those used in Fig.9.

Figure 11. The magnitudes of the two coefficients for a range of ka and d/a = 2.5. Solid line Eq.(59). Dashed line Eq.(58).

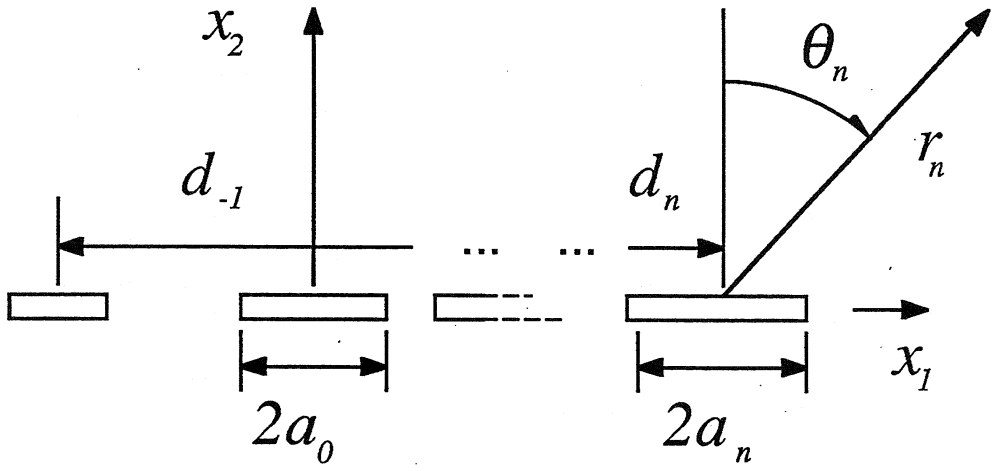

Fig. 1

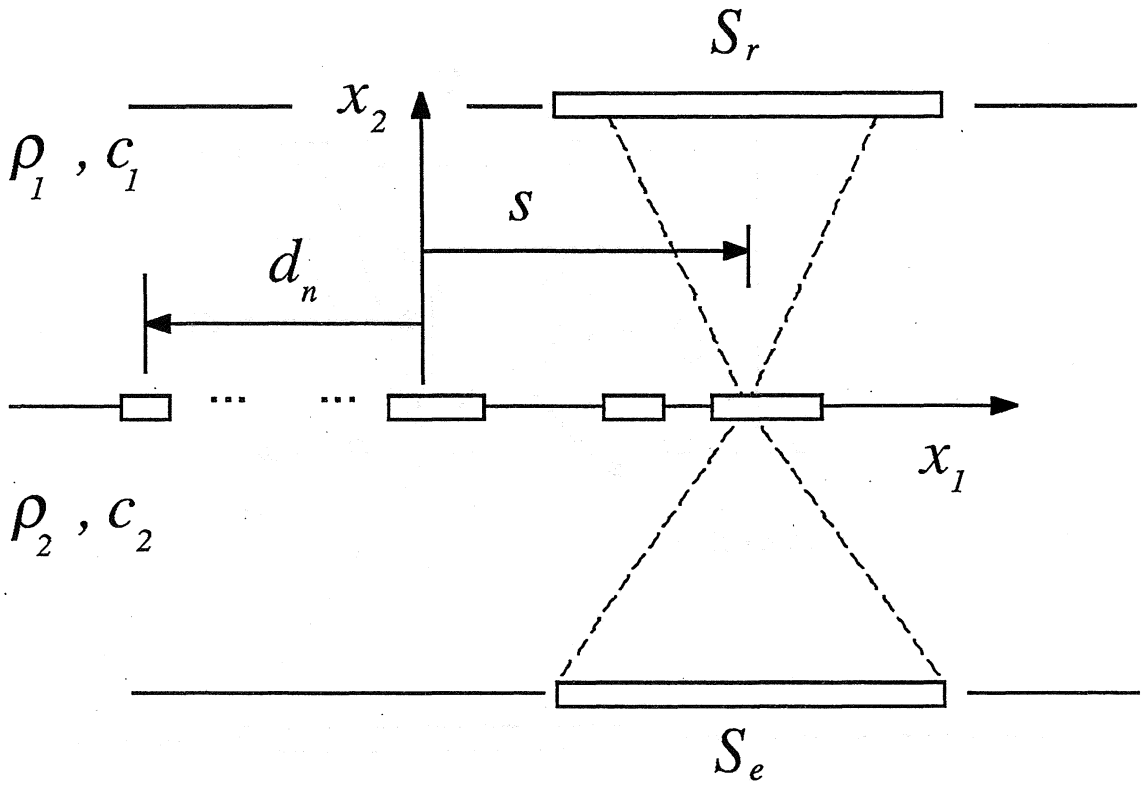

Fig. 2

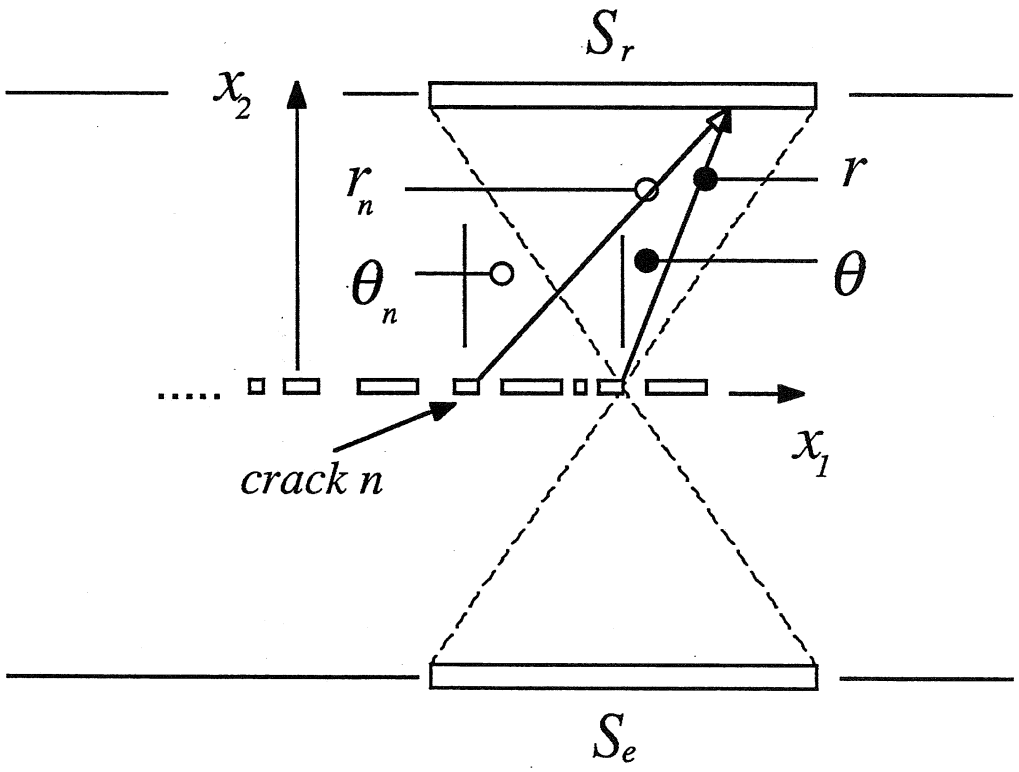

Fig. 3

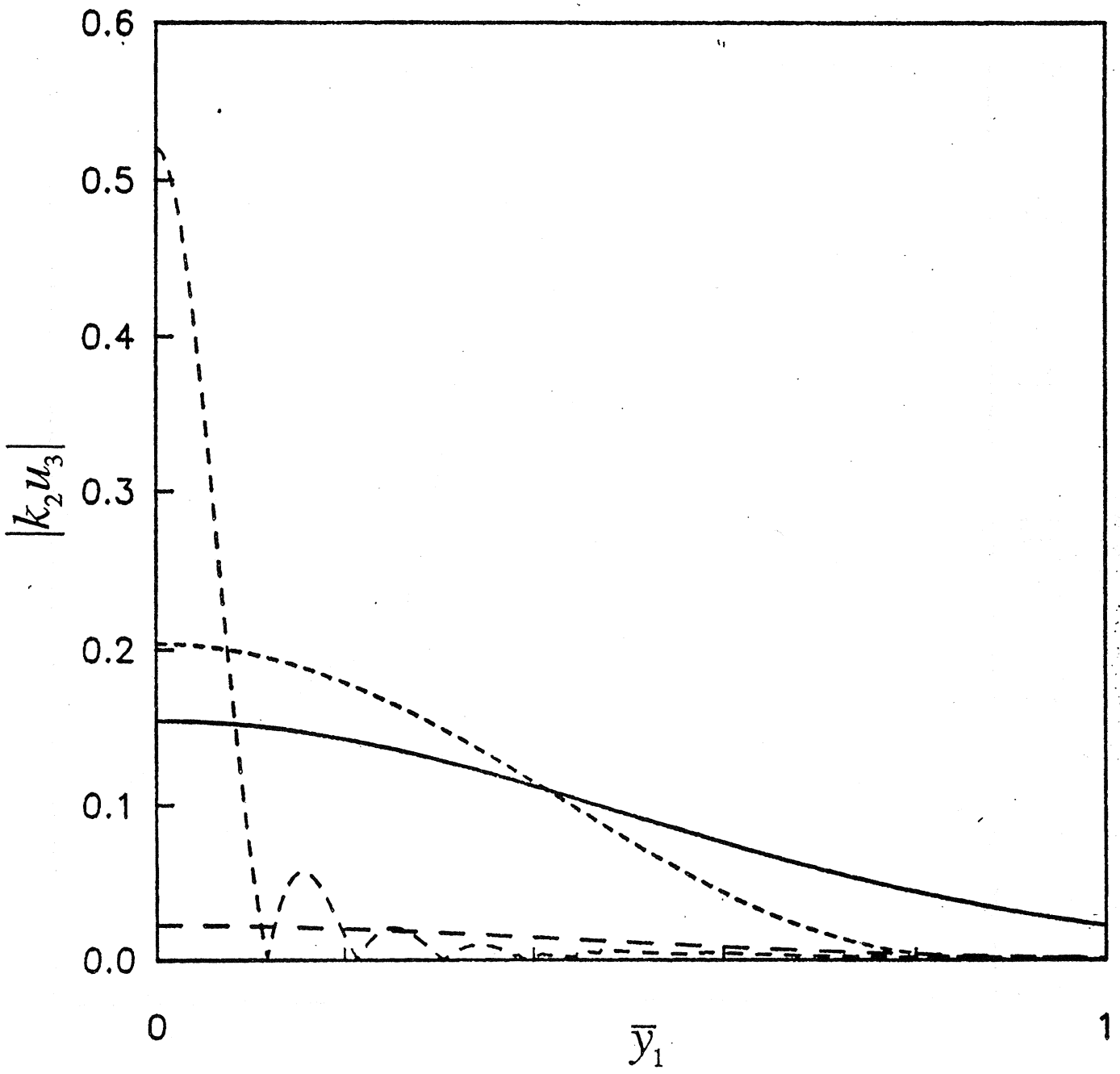

Fig. 4

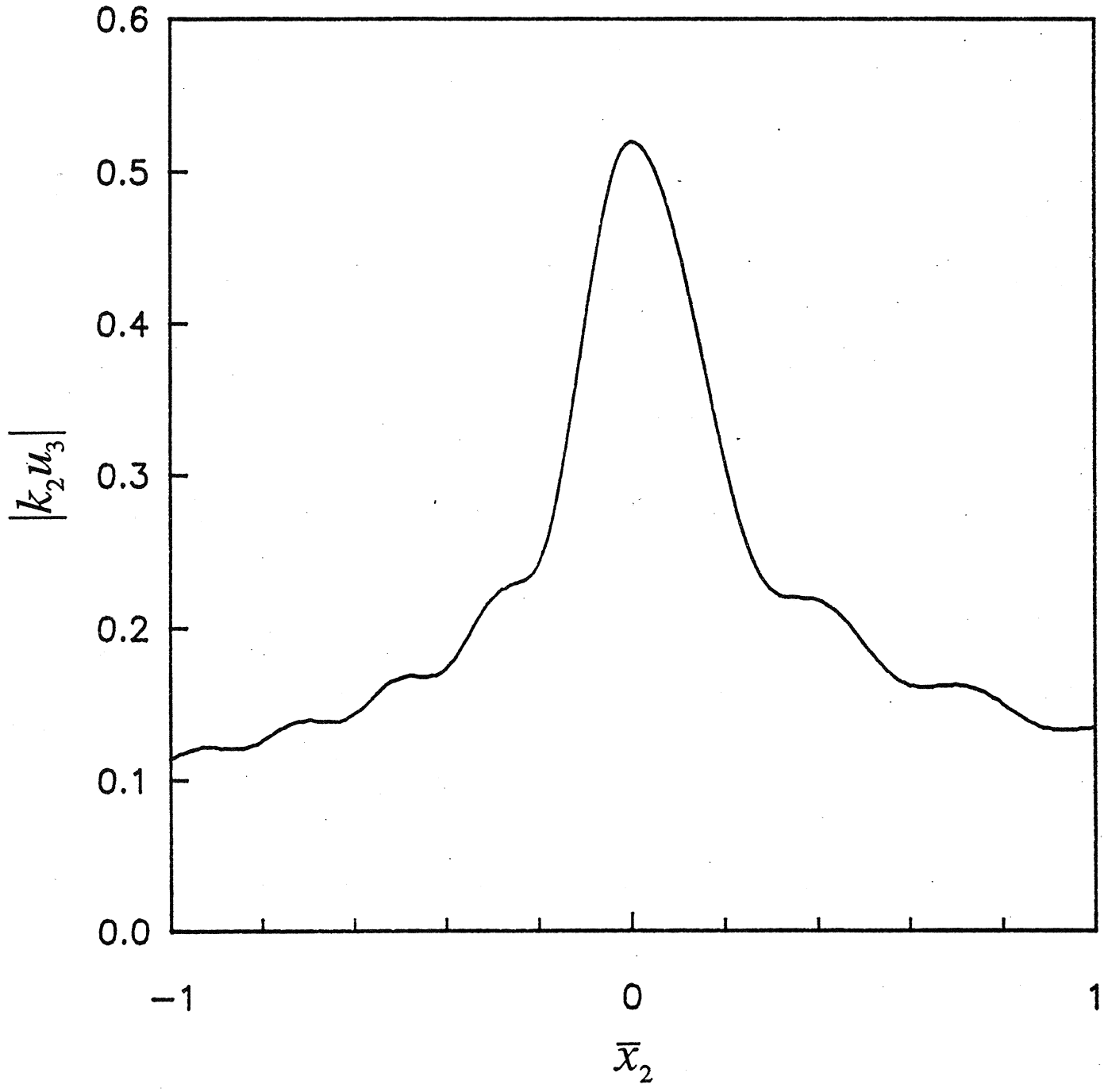

Fig. 5

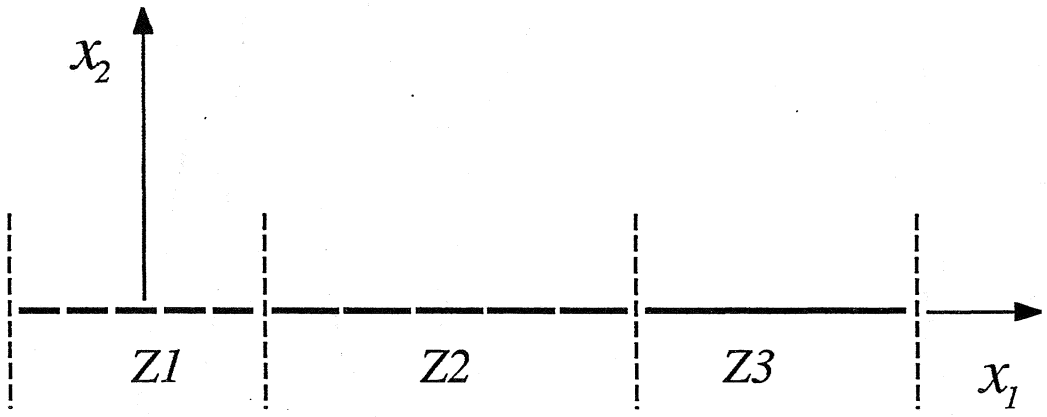

Fig. 6

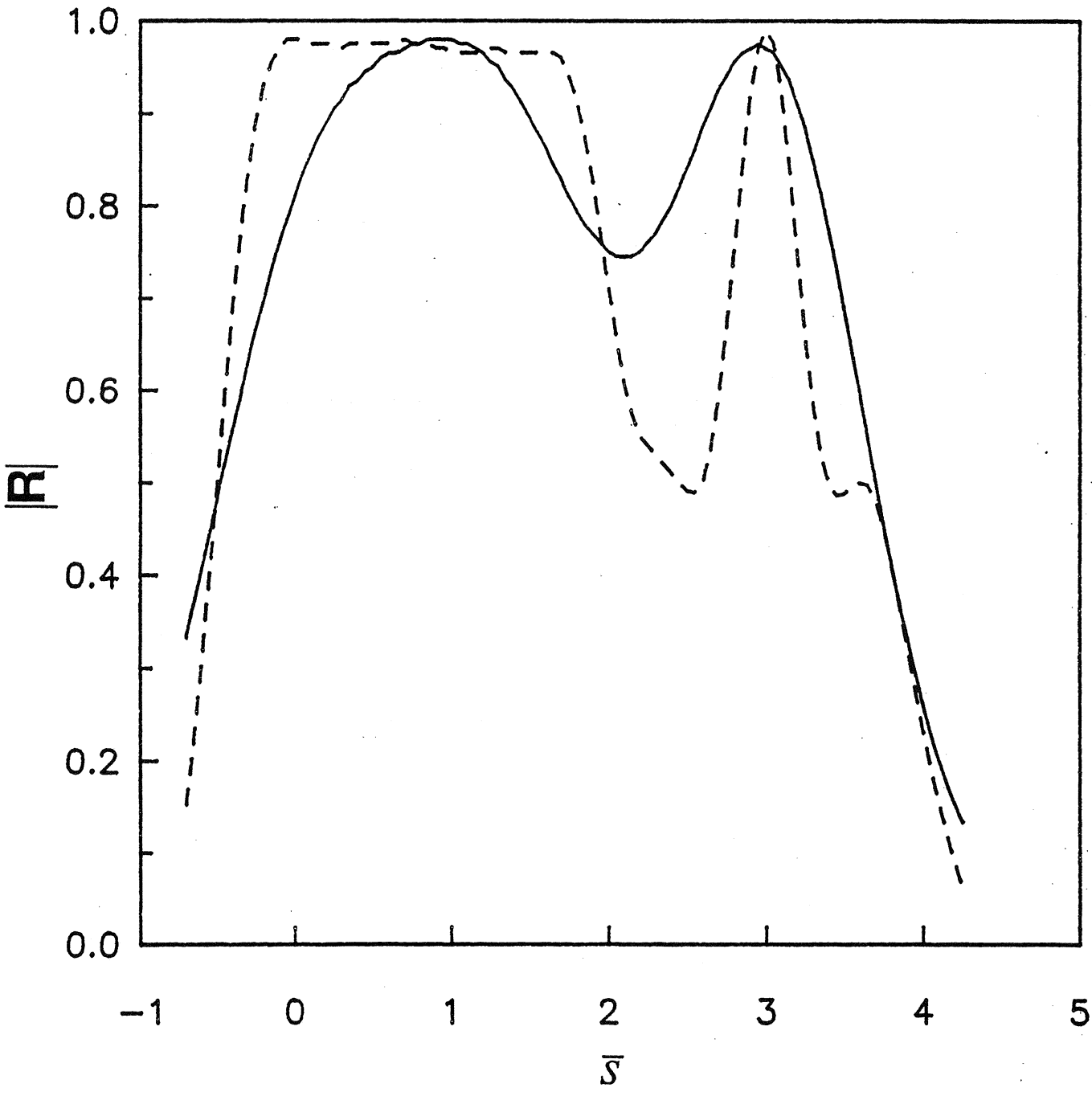

Fig. 7

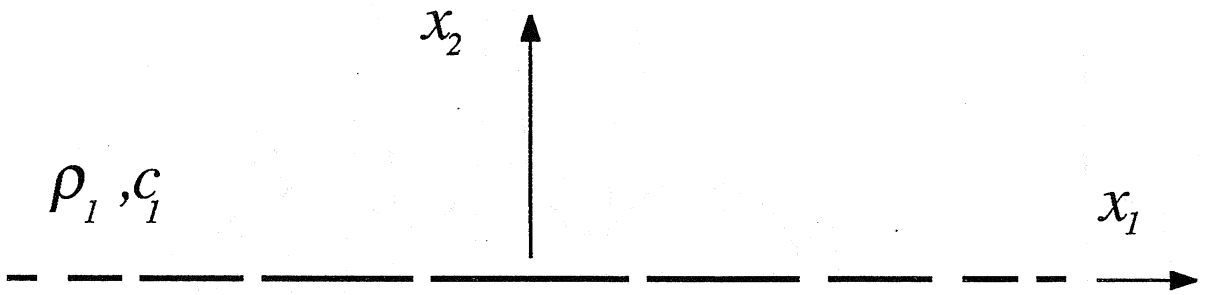

$$\bar{a}_n = 0.5 - 0.1n$$

$$|\bar{d}_n| = |\bar{d}_{n-1}| + \bar{a}_n + \bar{a}_{n-1} + 0.001$$

Fig. 8

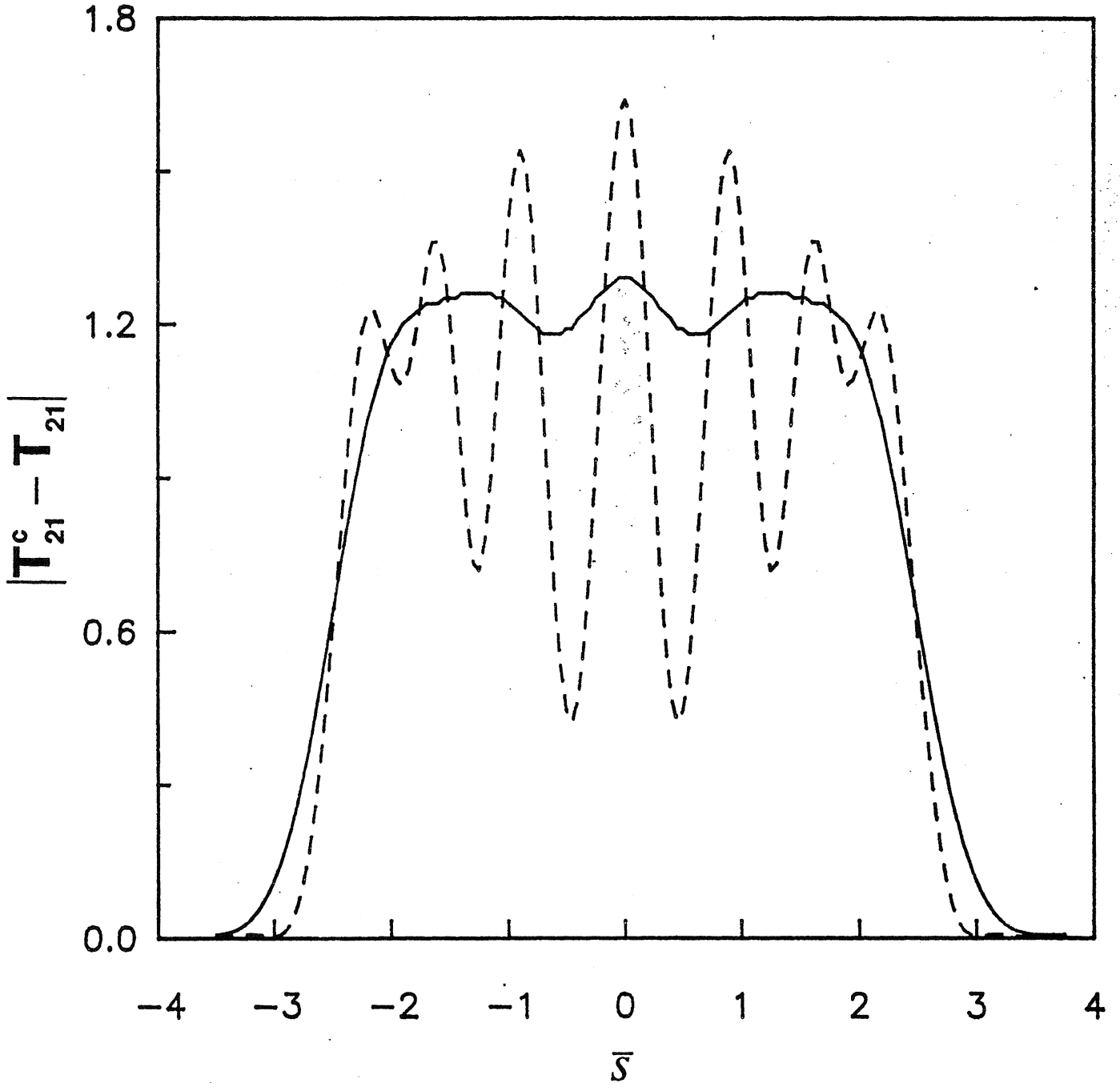

Fig. 9

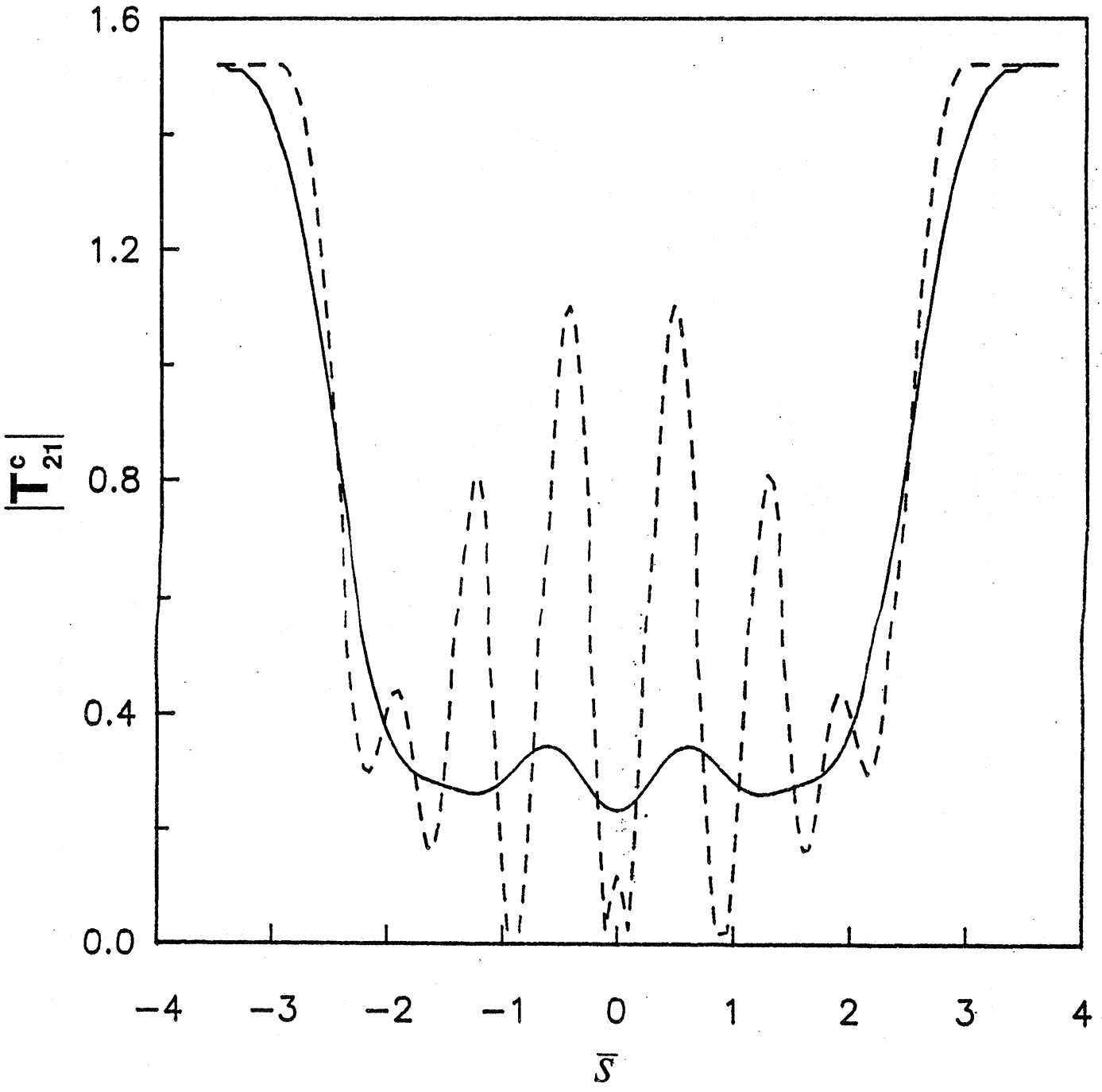

Fig. 10

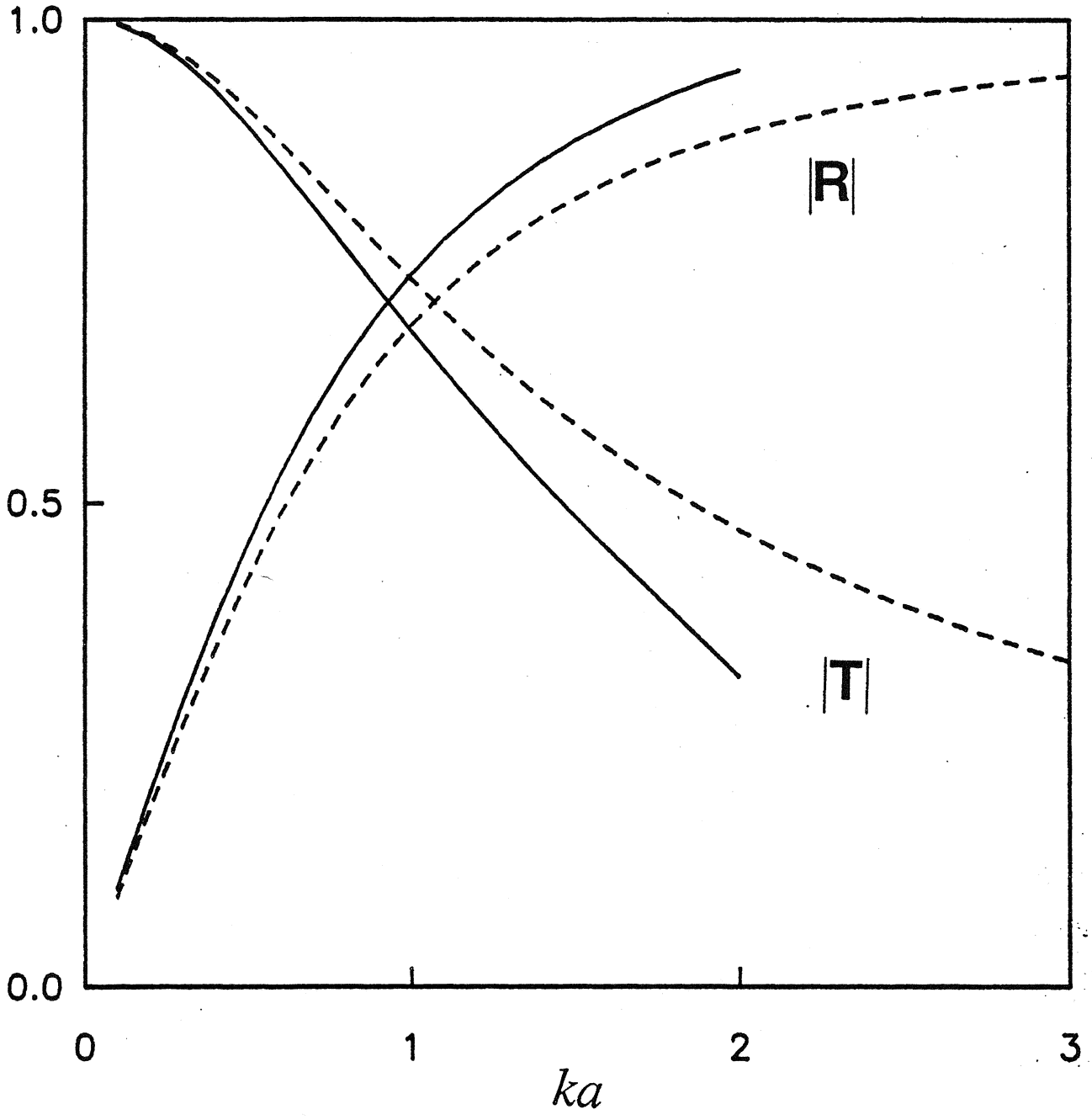

Fig. 11

List of Recent TAM Reports

No.	Authors	Title	Date
700	Juister, C. E., D. W. Newport, C. S. Payne, J. M. Peters, M. P. Thomas, and J. C. Trovillion	Twenty-seventh student symposium on engineering mechanics, M. E. Clark, coord. (1990)	Apr. 1992
701	Bernard, R. T., D. W. Claxon, J. A. Jones, V. R. Nitzsche, and M. T. Stadtherr	Twenty-eighth student symposium on engineering mechanics, M. E. Clark, coord. (1991)	Apr. 1992
702	Greening, L. E., P. J. Joyce, S. G. Martensen, M. D. Morley, J. M. Ockers, M. D. Taylor, and P. J. Walsh	Twenty-ninth student symposium on engineering mechanics, J. W. Phillips, coord. (1992)	May 1992
703	Kuah, H. T., and D. N. Riahi	Instabilities and transition to chaos in plane wakes	Nov. 1992
704	Stewart, D. S., K. Prasad, and B. W. Asay	Simplified modeling of transition to detonation in porous energetic materials	Nov. 1992
705	Stewart, D. S., and J. B. Bdzil	Asymptotics and multi-scale simulation in a numerical combustion laboratory	Jan. 1993
706	Hsia, K. J., Y.-B. Xin, and L. Lin	Numerical simulation of semi-crystalline Nylon 6: Elastic constants of crystalline and amorphous parts	Jan. 1993
707	Hsia, K. J., and J. Q. Huang	Curvature effects on compressive failure strength of long fiber composite laminates	Jan. 1993
708	Jog, C. S., R. B. Haber, and M. P. Bendsoe	Topology design with optimized, self-adaptive materials	Mar. 1993
709	Barkey, M. E., D. F. Socie, and K. J. Hsia	A yield surface approach to the estimation of notch strains for proportional and nonproportional cyclic loading	Apr. 1993
710	Feldsien, T. M., A. D. Friend, G. S. Gehner, T. D. McCoy, K. V. Remmert, D. L. Riedl, P. L. Scheiberle, and J. W. Wu	Thirtieth student symposium on engineering mechanics, J. W. Phillips, coord. (1993)	Apr. 1993
711	Weaver, R. L.	Anderson localization in the time domain: Numerical studies of waves in two-dimensional disordered media	Apr. 1993
712	Cherukuri, H. P., and T. G. Shawki	An energy-based localization theory: Part I—Basic framework	Apr. 1993
713	Manring, N. D., and R. E. Johnson	Modeling a variable-displacement pump	June 1993
714	Birnbaum, H. K., and P. Sofronis	Hydrogen-enhanced localized plasticity—A mechanism for hydrogen-related fracture	July 1993
715	Balachandar, S., and M. R. Malik	Inviscid instability of streamwise corner flow	July 1993
716	Sofronis, P.	Linearized hydrogen elasticity	July 1993
717	Nitzsche, V. R., and K. J. Hsia	Modelling of dislocation mobility controlled brittle-to-ductile transition	July 1993
718	Hsia, K. J., and A. S. Argon	Experimental study of the mechanisms of brittle-to-ductile transition of cleavage fracture in silicon single crystals	July 1993
719	Cherukuri, H. P., and T. G. Shawki	An energy-based localization theory: Part II—Effects of the diffusion, inertia and dissipation numbers	Aug. 1993
720	Aref, H., and S. W. Jones	Chaotic motion of a solid through ideal fluid	Aug. 1993
721	Stewart, D. S.	Lectures on detonation physics: Introduction to the theory of detonation shock dynamics	Aug. 1993
722	Lawrence, C. J., and R. Mei	Long-time behavior of the drag on a body in impulsive motion	Sept. 1993
723	Mei, R., J. F. Klausner, and C. J. Lawrence	A note on the history force on a spherical bubble at finite Reynolds number	Sept. 1993
724	Qi, Q., R. E. Johnson, and J. G. Harris	A re-examination of the boundary layer attenuation and acoustic streaming accompanying plane wave propagation in a circular tube	Sept. 1993
725	Turner, J. A., and R. L. Weaver	Radiative transfer of ultrasound	Sept. 1993
726	Yogeswaren, E. K., and J. G. Harris	A model of a confocal ultrasonic inspection system for interfaces	Sept. 1993